

can be used to investigate relaxation spectra in more complicated situations, for example in the presence of quadrupole interaction or an external magnetic field, if the directions of these fields coincide with the symmetry axes of the cube. The orders of the matrices to be inverted, however, doubles in comparison with the examples analyzed above.

<sup>1</sup>F. van der Woud and A. J. Dekker, Phys. Status Solidi 9, 775 (1965).

<sup>2</sup>H. H. Wickman, M. P. Klein, and D. A. Shirley, Phys. Rev.

152, 345 (1966).

<sup>3</sup>A. M. Afanas'ev and Yu. Kagan, Zh. Eksp. Teor. Fiz. 45, 1660 (1963) [Sov. Phys. -JETP 18, 1139 (1964)].

<sup>4</sup>Yu. Kagan and A. M. Afanas'ev, Zh. Eksp. Teor. Fiz. 47, 1108 (1964) [Sov. Phys. -JETP 20, 743 (1965)].

<sup>5</sup>H. Gabriel, Phys. Status Solidi 23, 195 (1967).

<sup>6</sup>H. Gabriel, J. Bosse, and K. Randar, Phys. Status Solidi 27, 301 (1968).

<sup>7</sup>M. Blume, Phys. Rev. 174, 351 (1968).

<sup>8</sup>L. L. Hirst, J. Phys. Chem. 31, 665 (1970).

<sup>9</sup>S. Dattagupta and M. Blume, Phys. Rev. B11, 4540 (1974).

<sup>10</sup>A. M. Afanas'ev and V. D. Gorobchenko, Zh. Eksp. Teor. Fiz. 66, 1406 (1974) [Sov. Phys. -JETP 39, 690 (1974)].

Translated by J. G. Adashko

## Magnetic transitions in mutual solid solutions of lower iron and manganese silicides

F. A. Sidorenko, Yu. A. Vereshchagin, E. N. Babanova, B. V. Ryzhenko, and P. V. Gel'd

Urals Polytechnic Institute, Sverdlovsk

(Submitted July 16, 1975)

Zh. Eksp. Teor. Fiz. 70, 628-638 (February 1976)

An investigation was made of the temperature dependences of the magnetization (4.2-900°K) and of the magnetic susceptibility (60-1200°K) of  $(\text{Fe}_{1-x}\text{Mn}_x)_3\text{Si}$  solid solutions ( $0 \leq x \leq 1$ ). The Mössbauer spectra of  $\text{Fe}^{57}$  in these solutions were recorded and a neutron diffraction study of their structure was made. The magnetic structures of the antiferromagnets  $\text{Mn}_3\text{Si}$  and  $(\text{Fe}_{0.33}\text{Mn}_{0.67})_3\text{Si}$  were determined. Three ranges of compositions were distinguished in the magnetic phase diagram: 1)  $0 \leq x < 0.33$ , 2)  $0.33 \leq x < 0.67$ , 3)  $0.67 \leq x \leq 1$ , in which the low-temperature order was, respectively, ferromagnetic, ferrimagnetic, and antiferromagnetic.

PACS numbers: 75.50.Ee, 75.25.+z, 75.30.Nc, 76.80.+y

### 1. INTRODUCTION

Magnetic properties and magnetic structure of many transition-metal alloys (such as Ni-Mn, Ni-Fe, and others) are governed by the competition between exchange interactions of opposite signs. It is interesting to determine the laws governing the magnetic structure of multicomponent systems, the simplest of which are quasibinary solid solutions with an ordered distribution of transition-metal atoms. An example of such solutions is the quasibinary  $(\text{Fe}_{1-x}\text{Mn}_x)_3\text{Si}$  system whose components  $\text{Fe}_3\text{Si}$  and  $\text{Mn}_3\text{Si}$  have the  $\text{D0}_3$  structure and an unlimited mutual solubility.

In an earlier paper<sup>[1]</sup> we showed that an increase of  $x$  from 0 to 0.33 in this system results in the replacement of iron atoms with Mn only at the  $C$  sites, whose immediate environment includes eight  $A$  and  $B$  sites occupied by iron atoms. Further increase of  $x$  is accompanied by the replacement of iron atoms at the  $A$  and  $B$  sites whose immediate environment includes four  $C$  sites occupied by manganese atoms and four  $D$  sites occupied by silicon.

The magnetic properties of these solutions were investigated in the composition ranges  $0 \leq x < 0.25$ <sup>[2]</sup> and  $0 \leq x < 0.6$ <sup>[3]</sup> but their magnetic structure was not inves-

tigated in detail. All that is known is that  $\text{Fe}_3\text{Si}$  is a collinear ferromagnet [ $\mu(\text{Fe}_C) = 2, 2\mu_B$  and  $\mu(\text{Fe}_{AB}) = 1, 15\mu_B$ ]<sup>[4]</sup> and  $\text{Mn}_3\text{Si}$  is an antiferromagnet (one of the variants of the magnetic structure of this antiferromagnet is described in<sup>[5]</sup>).

We investigated the influence of the composition ( $0 \leq x \leq 1$ ) and temperature of  $(\text{Fe}_{1-x}\text{Mn}_x)_3\text{Si}$  solid solutions on the magnetization (Sec. 3), magnetic susceptibility (Sec. 4), parameters of Mössbauer spectra (Sec. 5), and characteristics of magnetic scattering of neutrons (Sec. 6) with the aim of determining the conditions for the ferromagnetic-antiferromagnetic transition and the principal features of the magnetic phase diagram (Sec. 7).

### 2. SAMPLES AND INVESTIGATION METHODS

Our solid solutions were prepared from pure components (the impurity concentrations did not exceed 0.01% in iron, 0.02% in manganese, and 0.001% in silicon) in a hermetically sealed hf furnace and beryllium oxide crucibles. The melting and heat treatment conditions were described earlier.<sup>[1]</sup> A metallographic analysis demonstrated that samples of  $(\text{Fe}_{1-x}\text{Mn}_x)_3\text{Si}$  with  $0 \leq x \leq 0.6$  obtained in this way consisted of a single phase,

TABLE 1. Experimental values of ratios of (111) reflection intensities  $\gamma$  obtained at various temperatures and calculated (from these ratios) average magnetic moments  $\mu(\text{Fe/Mn})_C$  of atoms at C sites in  $(\text{Fe}_{1-x}\text{Mn}_x)_3\text{Si}$  solid solutions.

$x$	$T_1, ^\circ\text{K}$	$T_2, ^\circ\text{K}$	$\gamma = \frac{I_{111}^{T_1} K_1^*}{I_{111}^{T_2} K_1}$	$\mu(\text{Fe/Mn})_C$
0	293	893	1.45±0.03	2.3±0.1
0.05	293	873	2.16±0.5	2.3±0.1
0.10	293	873	7.0±0.5	2.1±0.2
0.17	293	723	17±2	1.7±0.3
0.20	77	623	3±0.5	2.0±0.2
0.28	77	623	1.35±0.03	2.0±0.2
0.33	77	293	1.16±0.03	1.8±0.1
0.40	77	293	1.12±0.03	1.5±0.1
0.45	77	293	1.11±0.03	1.3±0.1
0.50	77	293	1.11±0.03	1.3±0.1
0.55	77	293	1.09±0.03	1.1±0.2
0.60	77	293	1.04±0.03	0.9±0.2

\* $K_1$  and  $K_2$  are the temperature factors.

whereas those richer in manganese (with the exception of  $\text{Mn}_3\text{Si}$  and solutions of similar compositions) exhibited the presence of small amounts (< 2%) of the second phase which was most probably  $(\text{Mn}_{1-y}\text{Fe}_y)_5\text{Si}_3$ . X-ray spectroscopic microanalysis (carried out using a Cameca microprobe) revealed a slightly higher (2–5%) concentration of iron in these precipitates than in the matrix.

The method described was used to prepare two batches of samples: one was used in magnetic and neutron-diffraction investigations (Table 1) and the other, which was enriched with the  $\text{Fe}^{57}$  isotope, was used for Mössbauer spectroscopy.

The saturation magnetization was investigated in between 60 and 900 °K using a vibration magnetometer of the type described by Foner<sup>[6]</sup> and in the temperature range 4.2 to 78 °K we used a Domenicali pendulum magnetic balance. The maximum error in these measurements did not exceed 1–2%. We used spherical samples (of 2.5 mm in diameter) and also disk samples of 2 mm in diameter and 2 mm thick.

An investigation of the temperature dependence (60–1200 °K) of the magnetic susceptibility was carried out using a pendulum balance similar to that described in<sup>[7]</sup>; the error did not exceed 2%.

The Mössbauer spectra were obtained at 78 °K using annealed (for 12 h at 870 °K) powders (thickness 20–30 mg/cm<sup>2</sup>) and employing constant-velocity apparatus with an electrodynamic drive. The source was the  $\text{Co}^{57}$  isotope in a palladium matrix.

The neutron diffraction studies were carried out on samples described in<sup>[1]</sup>. Diffractograms were obtained using a beam of neutrons of  $\lambda = 1.07 \text{ \AA}$  wavelength at temperatures below and above the Curie or Néel temperature. Moreover, the ground magnetic state of solid solutions was determined by recording neutron diffraction patterns also at 4.2 °K.

### 3. MAGNETIZATION

Polytherms of the saturation magnetization  $\sigma(T)$  were investigated in fields of 6, 8, and 10.5 kOe. The results of measurements in  $H = 10.5 \text{ kOe}$  are plotted in

Fig. 1. As we can see, the solutions with  $x \leq 0.3$  have normal  $\sigma(T)$  curves which are described by the Bloch law at low temperatures. In the composition range  $x > 0.3$  there is an abrupt change in the nature of the dependences  $\sigma(T)$  and, particularly, a maximum appears near 60–70 °K, which is observed most clearly for  $(\text{Fe}_{0.60}\text{Mn}_{0.40})_3\text{Si}$ .

The magnetization curves  $\sigma(H)$  of the  $(\text{Fe}_{1-x}\text{Mn}_x)_3\text{Si}$  solutions with  $0 \leq x \leq 0.3$  were recorded at 65 °K, whereas those of the solutions with  $0.3 \leq x \leq 1$  were additionally determined at 4.2 °K. The nature of the dependences  $\sigma(H)$  enabled us to divide all the solid solutions into three groups. The solutions belonging to the first group ( $0 \leq x \leq 0.3$ ) were characterized by a ferromagnetic magnetization curve and by low paraprocess susceptibilities and saturation fields (2–3 kOe). Magnetic saturation was reached in the second group of solutions ( $0.33 \leq x < 0.66$ ) in fields of 3–5 kOe. Their saturation magnetization was considerably less than that of the iron-rich samples and the paraprocess susceptibility was higher. The manganese-rich solutions ( $0.6 < x \leq 1$ ) were characterized by a very small magnetic moment and linear dependences  $\sigma(H)$ .

The temperature and field dependences of the magnetization were used in the calculation of the Curie temperatures by the method of thermodynamic coefficients.<sup>[8]</sup>

The saturation magnetization at  $T = 4.2 \text{ °K}$  decreased steeply when  $x$  was increased from 0.3 to 0.4 and was practically the same for the solutions with  $x = 0.4$  and 0.5. The specific spontaneous magnetization was determined by extrapolation of the saturation magnetization to zero field and then to zero temperature in accordance with the  $T^{3/2}$  Bloch law for the samples with  $0 \leq x \leq 0.3$  and by the method of direct extrapolation for the solutions with  $0.33 \leq x \leq 0.6$ .

The average magnetic moments (Fig. 2) were calculated using the formula  $\bar{\mu} = \sigma_{00} M/nN$ , where  $M$  is the average molecular mass of  $(\text{Fe}_{1-x}\text{Mn}_x)_3\text{Si}$  solid solutions,  $N$  is the Avogadro number, and  $n$  is the number of mag-

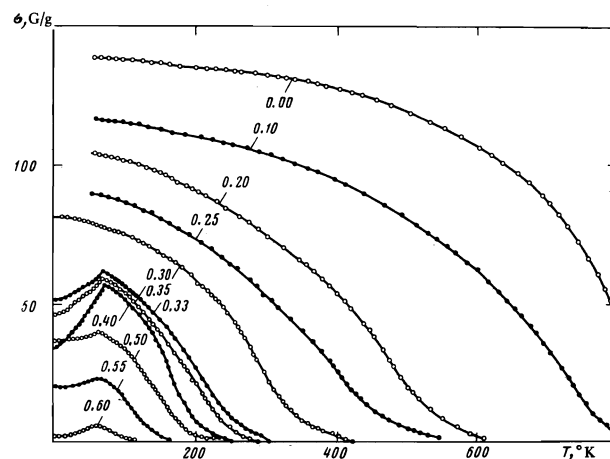


FIG. 1. Temperature dependences of the magnetization of  $(\text{Fe}_{1-x}\text{Mn}_x)_3\text{Si}$  solid solutions. The numbers alongside the curves give the values of  $x$ .

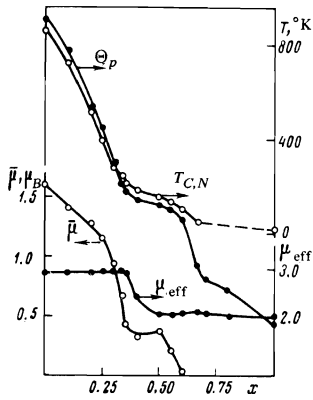


FIG. 2. Composition dependences of the average magnetic moment  $\bar{\mu}$ , effective magnetic moment  $\mu_{\text{eff}}$ , Curie and Néel temperatures  $T_{C,N}$ , and paramagnetic Curie temperature  $\Theta_p$ .

netic atoms in a nominal cell of  $\text{Mn}_3\text{Si}$  which is 3. It was found that the average magnetic moment per iron atom in  $\text{Fe}_3\text{Si}$  was  $1.61\mu_B$ , in good agreement with the results obtained earlier.<sup>[9]</sup> When iron was replaced with manganese, the average moment  $\bar{\mu}$  decreased particularly strongly in the range  $0.25 < x < 0.35$  whereas the changes in the  $0.35 \leq x \leq 0.50$  range were slight. However, the replacement of more than 50% of iron atoms with manganese again caused a rapid fall of  $\bar{\mu}$  to zero for  $(\text{Fe}_{0.33}\text{Mn}_{0.67})_3\text{Si}$  (Fig. 2). It should be pointed out that the recent<sup>[3]</sup> values of  $\bar{\mu}$  and  $T_C$  of  $(\text{Fe}_{1-x}\text{Mn}_x)_3\text{Si}$  samples quenched in water from  $800^\circ\text{C}$  were in reasonable agreement with our results obtained for samples that were annealed at  $950^\circ\text{C}$  and then cooled slowly.

#### 4. MAGNETIC SUSCEPTIBILITY

Polytherms of the magnetic susceptibility  $\chi(T)$  of solid solutions were described satisfactorily by Curie-Weiss law in the paramagnetic region. This made it possible to use the least-squares method in the calculation of the paramagnetic Curie temperature  $\Theta_p$ , Curie constant  $C$ , and effective magnetic moment  $\mu_{\text{eff}} = (3RC/N\mu_B)^{1/2}$  (Fig. 2).

The nature of the polytherms  $\chi(T)$  depended strongly on the composition. For example, in the case of the iron-rich solid solutions ( $0 \leq x < 0.33$ ) the dependence  $1/\chi(T)$  in the range  $T > T_C$  approached asymptotically a straight line  $1/\chi(T) = CT + \Theta_p$ , from above, which was typical of ferromagnetic materials, whereas in the case of the solutions richer in manganese ( $x > 0.33$ ) this dependence approached the asymptote from below, which was typical of ferrimagnets and antiferromagnets.

In the first group of solid solutions ( $0 \leq x < 0.33$ ) the effective magnetic moment of the metal atoms was practically independent of the composition and equal to  $2.9\mu_B$ . However, further replacement of iron atoms with manganese reduced this moment to  $2.4\mu_B$  and in the range  $0.5 < x \leq 1$  the magnetic moment again depended weakly on the composition. Up to  $x = 0.33$  the paramagnetic Curie temperature followed the variations of  $T_C$  remaining slightly above the latter. However, in the  $0.33 < x < 0.7$  range, this temperature became somewhat lower than  $T_C$  and at  $x > 0.66$  it changed its sign. This was a reliable indication of the antiferromagnetic nature of the manganese-rich alloys, which was pointed out by us (as mentioned in<sup>[3]</sup>) in earlier communications.

#### 5. MÖSSBAUER EFFECT

The Mössbauer spectra of some of the investigated  $(\text{Fe}_{1-x}\text{Mn}_x)_3\text{Si}$  solutions, normalized to infinity, and the concentration dependences of the effective fields at the  $\text{Fe}^{57}$  nuclei (extrapolated to absolute zero) are plotted in Fig. 3. The spectrum of the silicide  $\text{Fe}_3\text{Si}$  was the result of superposition of two hyperfine splitting lines, corresponding to two structurally inequivalent positions of iron atoms. The calculated values of the fields in nuclei of these atoms  $H(\text{Fe}_{AB}) = 215 \text{ kOe}$  and  $H(\text{Fe}_C) = 340 \text{ kOe}$  were in good agreement with the results reported in<sup>[10,11]</sup>. A weak ( $\sim 3\%$  of the amplitude of the absorption lines associated with  $\text{Fe}_{AB}$ ) third sextet was clearly due to incomplete ordering of the solutions.

All the absorption curves of the iron-rich  $(\text{Fe}_{1-x}\text{Mn}_x)_3\text{Si}$  solutions ( $0 \leq x < 0.33$ ) also exhibited a complex hyperfine structure. In the case of the solutions with small amounts of manganese, the sextets corresponding to the strongest internal field were related, as above, to the absorption of the  $\gamma$  rays by the  $\text{Fe}_C$  nuclei, as indicated also by a reduction in the amplitude of these peaks with rising  $x$ , in agreement with the sequence of replacement of the iron with manganese atoms established earlier.<sup>[1]</sup> Moreover, the absorption lines corresponding to  $\text{Fe}_{AB}$  were identified reliably.

The spectra of the samples with  $0.20 \leq x \leq 0.33$  were very complex. However, once again we observed that, as  $x$  was increased, the resonance absorption peaks became broader and both the splitting of the individual sextets and the intensities of the peaks associated with the  $\text{Fe}_C$  nuclei decreased.

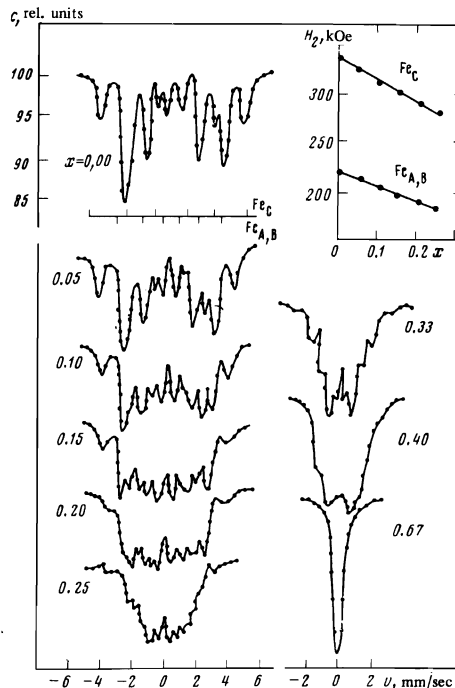


FIG. 3. Mössbauer spectra of  $(\text{Fe}_{1-x}\text{Mn}_x)_3\text{Si}$  solutions at  $78^\circ\text{K}$  and composition dependences of the effective magnetic fields at the  $\text{Fe}^{57}$  nuclei. The numbers alongside the curves give the values of  $x$ .

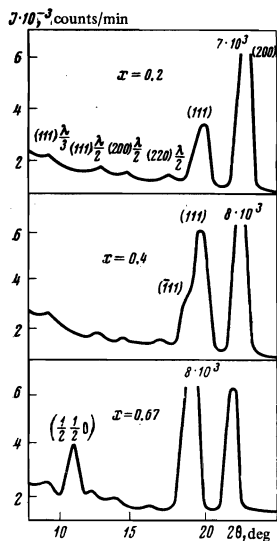


FIG. 4. Neutron diffraction patterns of  $(\text{Fe}_{1-x}\text{Mn}_x)_3\text{Si}$  solid solutions at 4.2 °K.

The spectra recorded for the  $0.45 < x < 0.67$  samples at 78 °K were single lines broadened because of the small difference between the Curie temperature  $T_C$  and the temperature at which these spectra were recorded. Moreover, the spectra of the samples with  $x = 0.67$  and  $x = 0.97$  were similar but the line widths were closer to the natural value.

The calculated effective field at the  $\text{Fe}^{57}$  nuclei in the  $0 \leq x \leq 0.25$  samples varied linearly from 215 to 164 kOe for  $\text{Fe}_{AB}^{57}$  and from 340 to 270 kOe for  $\text{Fe}_C^{57}$ , which was correlated with the linear variation of the average magnetic moment.

## 6. NEUTRON DIFFRACTION ANALYSIS

The nature of the magnetic order was determined by recording neutron diffraction patterns of 12 samples of  $(\text{Fe}_{1-x}\text{Mn}_x)_3\text{Si}$  solutions whose compositions are listed in Table 1 together with the data on the conditions under which these patterns were recorded.

In the angular range  $3 < 2\theta < 35^\circ$  there were three nuclear reflections (111), (200), and (220) in the neutron diffraction patterns of all the compositions recorded at temperatures  $T_2 > T_{C,N}$ .

The diffraction patterns recorded at temperatures  $T_1 < T_{C,N}$  were basically identical for each group of samples. The patterns obtained for the first group ( $0 \leq x < 0.33$ ) had three magnetic reflections (111), (200), and (220) at temperatures below  $T_C$  (Fig. 4) and these were superimposed on the nuclear reflections (Fig. 4a) of which the first was the strongest. Within the limits of the experimental error, the magnetic contributions to all these reflections depended weakly on the composition.

The neutron diffraction patterns of the solutions with  $0.03 \leq x < 0.67$  (Fig. 4) recorded at 78 °K (which was slightly less than the temperature of the transition to the paramagnetic state) differed from those described above because an increase in the manganese content reduced strongly the intensity of the magnetic contribution to the (111) reflection. When temperature was reduced to 4.2 °K, this reflection split into two: (111)

and  $(\bar{1}11)$ . This splitting of the (111) line was explained by the rhombohedral distortion of the unit cell, which was strongest for  $x = 0.40$  ( $\alpha = 88^\circ 16'$ ) and decreased to zero when  $x$  was increased from 0.50 ( $\alpha = 88^\circ 26'$ ) to 0.67 ( $\alpha = 90^\circ$ ).

The diffraction patterns of the samples with  $0.67 \leq x \leq 1$  recorded at 78 °K had no magnetic reflections but at 4.2 °K there were magnetic reflections of the  $(\frac{1}{2}\frac{1}{2}0)$  and (100) types (Fig. 4).

Magnetic contributions to the Bragg peaks were separated using the ratios of the intensities of the reflections obtained at different temperatures  $T_1$  and  $T_2$  allowing for the Debye factor. The Debye temperatures, estimated from the elastic constants, were close to  $470 \pm 20^\circ \text{K}$  for all the investigated solutions. Table 1 gives the values of the ratios  $\gamma = I_{(111)}^{T_1} / I_{(111)}^{T_2}$  ( $T_1 < T_C < T_2$ ) and the magnetic moments of the atoms at the C sites deduced from these ratios. The values of  $\gamma$  for the (200) and (220) lines were not used in the calculations because the magnetic contributions to these reflections were very small. The replacement of iron at the C sites with manganese in the  $0 \leq x < 0.33$  range did not alter significantly the magnetic moment  $\mu(\text{Fe}_C, \text{Mn}_C)$ , which was  $(2.3 \pm 0.1)\mu_B$  for  $\text{Fe}_3\text{Si}$  and  $(2.0 \pm 0.1)\mu_B$  for the solution with  $x = 0.28$ . In the case of the solution with  $x = 0.33$  the magnetic moment  $\mu(\text{Mn}_C)$  was  $(1.8 \pm 0.1)\mu_B$ . However, a further increase of  $x$  reduced the magnetic moment of the manganese atoms at the C sites to  $0.9\mu_B$  for  $x = 0.6$ .

A comparison of the calculated and experimentally determined intensities of the (111) and  $(\bar{1}11)$  reflections of the sample with  $x = 0.4$  indicated that the magnetic moment of the manganese atoms  $\text{Mn}_C$  at 4.2 °K was oriented parallel to the rhombohedral axis.

## 7. MAGNETIC STRUCTURE OF $(\text{Fe}_{1-x}\text{Mn}_x)_3\text{Si}$ SOLUTIONS

An analysis of the above experimental results leads, first of all, to the conclusion that variation of the composition of the  $(\text{Fe}_{1-x}\text{Mn}_x)_3\text{Si}$  solid solutions results in a transition from the ferromagnetic state typical of  $\text{Fe}_3\text{Si}$  to the antiferromagnetic state of  $\text{Mn}_3\text{Si}$  via a series of intermediate magnetic structures. The magnetic phase diagram of the investigated solid-solution system (Fig. 5) can be divided into at least four regions: I) ferromagnetic states; II) ferrimagnetic states; III) antiferromagnetic states; IV) paramagnetic states.

We shall now consider possible mechanisms of the formation of the various magnetic states in each of the three groups of alloys discussed above.

1. *Ferromagnetic solutions with  $0 \leq x < 0.33$ .* We recall that in the investigated solid solutions the replacement of iron with manganese does not alter basically the neutron diffraction pattern and the magnetic moment of the metal atoms located at the C sites remains fairly large for all compositions. In the same composition range the Curie temperature  $T_C$  falls steeply and there is a strong reduction in the average magnetic moment (from  $1.16\mu_B$  for  $x = 0$  to  $1\mu_B$  for  $x = 0.3$ ). Clearly, this can be regarded as evidence of

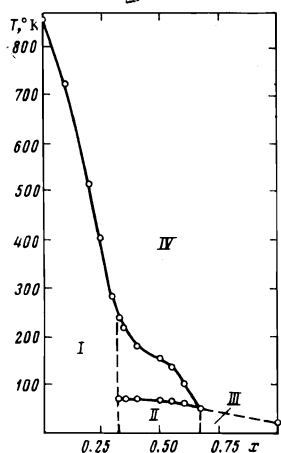


FIG. 5. Magnetic phase diagram of the  $(\text{Fe}_{1-x}\text{Mn}_x)_3\text{Si}$  solid-solution system.

a reduction in the projection of the magnetic moment along the spontaneous magnetization direction. This is supported also by the results obtained from the Mössbauer spectra. This reduction in the  $z$  projections of the moments does not necessarily represent a reduction in the intrinsic moments, especially as the Mn atoms at the  $C$  sites have a large magnetic moment that differs from that of the iron atoms  $\text{Fe}_C$  (see Table 1). This is further supported also by the constancy of the effective magnetic moment. A magnetic state of this kind is clearly the result of competition between exchange interactions of opposite signs (for example,  $I_{\text{Fe-Fe}} > 0$ ,  $I_{\text{Fe-Mn}} > 0$ ,  $I_{\text{Mn-Mn}} < 0$ ), which may produce a canted magnetic structure or an additional quantum precession in which collinearity is retained.

2. *Solutions with intermediate magnetic structure* ( $0.33 \leq x < 0.67$ ). In considering the various magnetic configurations of our solid solutions we shall take into account the following properties: the extremal temperature dependence of the magnetization (Fig. 1), the fall of the paramagnetic temperature relative to the Curie point which becomes greater with increasing manganese concentration, and antiferromagnetism of  $(\text{Fe}_{0.33}\text{Mn}_{0.67})_3\text{Si}$ .

As pointed out earlier (Sec. 1), the number of manganese atoms at the  $A$  and  $B$  sites increases in compositions with more than 33 mol. %  $\text{Mn}_3\text{Si}$ . If the magnetic interaction of the  $\text{Mn}_{AB}$  and  $\text{Mn}_C$  atoms, which are separated by shortest distances, is sufficiently strong and negative, the directions of the magnetic moments of the first manganese atoms replacing iron at the  $AB$  sites is opposite to the direction of the magnetic moments of the nearest neighbors of  $\text{Mn}_C$ . This means that the new structure is ferrimagnetic and one of its characteristic temperatures corresponds to the extremum of the dependence  $\sigma(T)$  (Fig. 1). It remains unclear whether the magnetic moment of any one of the atoms ( $\text{Mn}_{AB}$  or  $\text{Mn}_C$ ) has a component directed opposite to the main ferromagnetic moment of the matrix. As  $x$  is increased ( $> 0.33$ ), the number of  $\text{Mn}_C$ - $\text{Mn}_{AB}$  pairs increases, which is responsible for the observed growth of ferrimagnetism. This is in agreement with the observed fall of the paramagnetic temperature compared with the Curie temperature.

In accordance with the initial assumption about the signs of the exchange interactions, the second manganese atoms reaching the  $A$ - $B$  sublattice participate immediately in three interactions: the negative interactions with the neighboring  $\text{Mn}_C$  and  $\text{Mn}_{AB}$  atoms, and the positive interaction with  $\text{Fe}_{AB}$ . The first two represent an increase in the magnetic energy of a crystal with any fixed magnetic temperature. Clearly, this is why the ferrimagnetic component is observed most clearly for the solution with  $x = 0.42$ , for which the probability of finding just one  $\text{Mn}_{AB}$  atom near  $\text{Mn}_C$  reaches its maximum value. An increase in  $x$  above 0.42 results in a strong increase of the statistical weight of the configurations with two or more  $\text{Mn}_{AB}$  atoms near an atom of  $\text{Mn}_C$ , which reduces the ferrimagnetic component.

As  $x$  is increased from 0.42 to 0.67, the negative contribution to the  $0^\circ\text{K}$  magnetization gradually changes to the antiferromagnetic compensation of the sublattices, which reduces the magnetization fields at the  $\text{Fe}^{57}$  nuclei, reverses the sign of  $\Theta_p$ , and finally results in complete antiferromagnetic compensation of the sublattices (when  $x = 0.67$  is reached). At the same time the rhombohedral distortion of the lattice decreases.

This growth of antiferromagnetism does not have a purely magnetic manifestation because of the random distribution of manganese and iron atoms between the sites in the  $A$ - $B$  sublattice.

3. *Antiferromagnetic solid solutions.* The magnetic reflections  $(\frac{1}{2}\ 0\ 0)$  and  $(100)$  found in the neutron diffraction patterns of the manganese-rich alloys recorded at  $4.2^\circ\text{K}$  are evidence of the antiferromagnetic order. The magnetic cell formed in this process is at least twice as large as the chemical cell.

An analysis of a cell of this kind in the case of the silicide  $\text{Mn}_3\text{Si}$  shows that there can be two similar structures, both of which ensure that the calculated and observed intensities are in agreement. One of these is described in<sup>[5]</sup> and the other is shown in Fig. 6a, where the magnetic order is shown only within one chemical cell. This model presupposes the existence of four magnetic sublattices. Two of them are associated with  $\text{Mn}_{AB}$  atoms, the other two with  $\text{Mn}_C$ . The magnetic moments of the  $\text{Mn}_{AB}$  atoms are oriented in such a way that they interact ferromagnetically in planes parallel to  $(100)$ , whereas the coupling between these planes is antiferromagnetic. The  $\text{Mn}_C$  atoms interact ferromag-

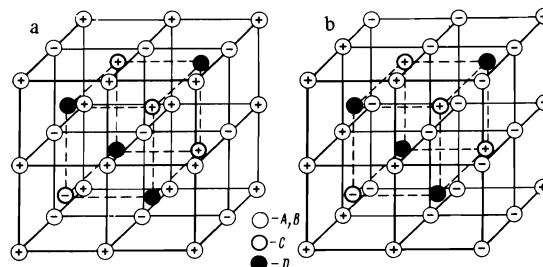


FIG. 6. Magnetic order in a chemical cell of the silicide  $\text{Mn}_3\text{Si}$  (a) and in the solid solution  $(\text{Fe}_{0.33}\text{Mn}_{0.67})_3\text{Si}$  (b).

netically in (110) layers and antiferromagnetically along directions normal to these layers. However, atoms of both types interact ferromagnetically along [100].

The intensities of the magnetic peaks ( $\frac{1}{2}\frac{1}{2}0$ ) and (100), normalized to the intensity of the pure nuclear reflection (111), enabled us to estimate the magnetic moments of the manganese atoms located at different sites:

$$\mu(\text{Mn}_{AB}) = (0,5 \pm 0,1) \mu_B \quad \mu(\text{Mn}_C) = (0,6 \pm 0,1) \mu_B$$

A structure of the silicide  $\text{Mn}_3\text{Si}$  slightly different from that shown in Fig. 6a<sup>[5]</sup> gives, for the same value of  $\mu(\text{Mn}_{AB})$ , the magnetic moment  $\mu(\text{Mn}_C) = (0,8 \pm 0,1) \mu_B$ . However, in both structures the magnetic moment of  $\text{Mn}_C$  is greater than the moment of  $\text{Mn}_{AB}$ , as found also for iron atoms ( $\text{Fe}_C$  and  $\text{Fe}_{AB}$ ) in the silicide  $\text{Fe}_3\text{Si}$ .<sup>[4]</sup>

The neutron diffraction pattern of  $(\text{Fe}_{0,33}\text{Mn}_{0,67})_3\text{Si}$  obtained at 4.2 °K has only one magnetic reflection ( $\frac{1}{2}\frac{1}{2}0$ ), whose relative intensity is much higher than in the diffraction spectrum of  $\text{Mn}_3\text{Si}$ . This is most likely due to the magnetic contribution of all the iron and manganese magnetic sublattices to the ( $\frac{1}{2}\frac{1}{2}0$ ) reflection. The relevant structure is shown in Fig. 6b. Since the distribution of the iron and manganese atoms in the A-B sublattice is random,<sup>[1]</sup> Fig. 6b shows only a general distribution of spins between these sites, corresponding to the ( $\frac{1}{2}\frac{1}{2}0$ ) reflection. The magnetic moments of the manganese atoms at the C sites are oriented antiparallel to one another along the [100] directions and each of these moments is opposite to the total magnetization of the nearest neighbors at the A and B sites.

This magnetic structure of  $(\text{Fe}_{0,33}\text{Mn}_{0,67})_3\text{Si}$  is similar to the magnetic structure of  $\text{Mn}_3\text{Si}$  shown in Fig. 6b, so that we can give preference to the latter compared with the silicide structure proposed in the model used in<sup>[5]</sup>.

Unfortunately, the available information is insufficient for the calculation of the partial magnetic moments of the iron and manganese atoms because only one magnetic reflection is found in the neutron diffraction pattern.

Continuous variation of the magnetic disordering temperature in the composition range  $0,67 < x < 1,00$  can be regarded as additional evidence—as demonstrated by Kalishevich and Lutskaya (to be published separately)—of the similarity of the magnetic structures of the  $(\text{Fe}_{0,33}\text{Mn}_{0,67})_3\text{Si}$  and  $\text{Mn}_3\text{Si}$  silicides. This is most probably why the solid solutions retain the ferromagnetic distribution of the magnetic moments of  $\text{Mn}_C$  in the (110) planes and the ferromagnetic interaction of atoms of all kinds along the [100] direction.

An analysis of the expressions for the exchange energy of the antiferromagnets of the type described above shows that this energy is governed by the competition between the exchange interactions in the various coordination spheres. In the case of  $\text{Mn}_3\text{Si}$  and  $(\text{Fe}_{0,33}\text{Mn}_{0,67})_3\text{Si}$  the expressions for the interaction energy obtained allowing for the orientations of the magnetic moments within three coordination spheres are as follows:

$$\text{Mn}_3\text{Si} - E_{\text{exch}} \approx -32I^I(\text{Mn}_{AB} - \text{Mn}_C)S(\text{Mn}_{AB})S(\text{Mn}_C)$$

$$+32I^{II}(\text{Mn}_{AB} - \text{Mn}_{AB})S^2(\text{Mn}_{AB}) - 64I^{III}(\text{Mn}_{AB} - \text{M}_{AB})S^2(\text{Mn}_{AB});$$

$$(\text{Fe}_{0,33}\text{Mn}_{0,67})_3\text{Si} - E_{\text{exch}} \approx -32I^I((\text{Mn}/\text{Fe})_{AB} - \text{Mn}_C)$$

$$\times S((\text{Mn}/\text{Fe})_{AB})S(\text{Mn}_C) - 16I^I(\text{Mn}_C - (\text{Mn}/\text{Fe})_{AB})$$

$\times S(\text{Mn}_C)S((\text{Mn}/\text{Fe})_{AB}) + 32I^{II}((\text{Mn}/\text{Fe})_{AB} - (\text{Mn}/\text{Fe})_{AB})S^2((\text{Mn}/\text{Fe})_{AB})$ , where  $I$  are the exchange integrals and  $S$  are the values of the magnetic moments. These relationships are fairly formal, because the values of the exchange integrals which occur in them are not known. However, it follows from these expressions that the exchange energy of  $(\text{Fe}_{0,33}\text{Mn}_{0,67})_3\text{Si}$  is greater (in the absolute sense) than the corresponding energy of  $\text{Mn}_3\text{Si}$  (because the signs of the first and second terms are opposite in the case of  $\text{Mn}_3\text{Si}$ ). This should reduce the Néel temperature as a result of a change in the magnetic structure as  $x$  is increased from 0.67 to 1, which is indeed observed experimentally.

## CONCLUSIONS

1. The results of x-ray, neutron diffraction, and magnetic measurements, and also of a study of the Mössbauer spectra carried out in a wide temperature range (4.2–1000 °K) enabled us to construct and discuss the magnetic phase diagram of  $(\text{Fe}_{1-x}\text{Mn}_x)_3\text{Si}$  solid solutions. In particular, we demonstrated that these solutions exhibit a ferro-ferri-antiferromagnetic series of transitions when the composition is varied. The low-temperature magnetic properties made it possible to divide the  $(\text{Fe}_{1-x}\text{Mn}_x)_3\text{Si}$  solid solutions into three groups: a) ferromagnetic ( $0 \leq x < 0,33$ ); b) ferrimagnetic ( $0,33 \leq x < 0,67$ ); c) antiferromagnetic ( $0,67 \leq x \leq 1$ ).

2. We considered the influence of composition on the magnetic order and nature of the exchange coupling between iron and manganese atoms in  $(\text{Fe}_{1-x}\text{Mn}_x)_3\text{Si}$ . The results obtained indicated that in the  $0 \leq x < 0,33$  range the magnetic structure formation was dominated by the positive exchange interactions of the Fe-Fe and Fe-Mn type. At high manganese concentrations ( $0,67 \leq x \leq 1$ ) the antiferromagnetic order was established because of the strong negative interaction between neighboring manganese atoms. Finally, in the intermediate range of manganese concentrations ( $0,33 < x < 0,67$ ) the solid solutions exhibited a complex ferrimagnetic structure whose appearance was clearly due to the competition between the above-mentioned positive and negative exchange interactions.

<sup>1</sup>E. N. Babanova, F. A. Sidorenko, P. V. Gel'd, and N. I. Basov, Fiz. Metal. Metalloved. **36**, 586 (1974).

<sup>2</sup>J. G. Booth, J. E. Clark, P. J. Webster, and S. Yoon, Proc. Intern. Conf. on Magnetism, Moscow, 1973, Vol. 4, VINITI, Moscow, 1974, p. 577.

<sup>3</sup>S. Yoon and J. G. Booth, Phys. Lett. A **48**, 381 (1974).

<sup>4</sup>D. Meinhardt and O. Krisement, Z. Phys. **174**, 472 (1963).

<sup>5</sup>E. N. Babanova, F. A. Sidorenko, and P. V. Gel'd, Fiz. Tverd. Tela (Leningrad) **17**, 956 (1975) [Sov. Phys.-Solid State **17**, 616 (1975)].

<sup>6</sup>S. Foner, Rev. Sci. Instrum. **30**, 548 (1959).

<sup>7</sup>Yu. N. Tsiolkovkin and A. N. Bashkatov, Fizicheskie svoistva metallov i splavov (Physical Properties of Metals and Alloys), Tr. Ural. Politekh. Inst. No. 186, 194 (1970).

<sup>8</sup>K. P. Belov, Magnitnye prevrashcheniya, Fizmatgiz, M., 1959 (Magnetic Transitions, Consultants Bureau, New York,

1961).

<sup>9</sup>P. Lecocq and A. Michel, C. R. Acad. Sci. 256, 1817 (1964).

<sup>10</sup>T. Shinjo, Y. Nakamura, and N. Shikazono, J. Phys. Soc. Jpn. 18, 797 (1963).

<sup>11</sup>R. Nathans, M. T. Pigott, and C. G. Shull, J. Phys. Chem. Solids 6, 38 (1958).

Translated by A. Tybulewicz

# Surface quantum spin waves in a degenerate electron liquid in metals in a weak magnetic field

V. P. Silin and O. M. Tolkachev

*P. N. Lebedev Physical Institute, USSR Academy of Sciences*

(Submitted July 21, 1975)

Zh. Eksp. Teor. Fiz. 70, 639-656 (February 1976)

We have discovered a possibility of propagation of surface waves in metals with a cylindrical Fermi surface; this is due to the electron Fermi-liquid interaction. We evaluate in the framework of the theory of a degenerate Fermi liquid the frequency spectra and damping coefficients and find the conditions for the existence of such waves.

PACS numbers: 75.30. F

## 1. INTRODUCTION

It is well known<sup>[1]</sup> that the surface states of electrons which have a "glancing" motion along the surface of a metal determine the electromagnetic properties of metals in the uhf band ( $10^{10}$  to  $10^{11}$  Hz) in relatively weak magnetic fields (1 to 10 gauss). The centers of the Larmor orbits of the "glancing" electrons are distributed outside the metal at distances which are almost equal to the Larmor radius (Fig. 1) and in momentum space the motion of such electrons corresponds to a closed orbit which bounds the hashed segment (Fig. 2). Transitions between the levels of the surface states lead to resonance absorption of radiation which manifests itself in experimentally observed oscillations of the surface impedance of the metal.

The theoretical possibility of the existence of surface waves in metals with a cylindrical Fermi surface near frequencies of the resonance transition between surface levels was discovered in<sup>[2]</sup>. In the same paper the impossibility was pointed out of the propagation of surface waves in metals with a spherical Fermi surface. On the other hand, up to now the problem has not been raised about the occurrence of effects which are connected with the electron surface states and which are at the same time caused by interelectron correlations. We shall present in the present paper the results of a theory of spin waves in an electron liquid, which takes into account the effect of electron surface states. The behavior of the surface spin waves found below enables us to confirm that the electron-electron interaction is one of the general causes for the existence of different

kinds of surface waves and of the resonance properties of a metal near the frequencies of the electron transitions between surface levels. This enables us to disconnect the existence of absorption resonance and of surface waves from the necessity that there exist some particular shapes of the Fermi surface; this corresponds to a qualitative difference between the new kind of excitations which are considered by us and those predicted in<sup>[2]</sup>.

## 2. QUANTUM KINETIC EQUATION

To solve the problem in which we are interested we must first of all carry out a generalization of the quantum kinetic equation of a degenerate electron liquid (see, e.g.,<sup>[3]</sup>), taking into account the role of the electron surface levels. Bearing in mind that an electron state is characterized by a set of quantum numbers  $\nu$  and assuming that the density matrix of the ground state of the electrons is diagonal we can write down the non-equilibrium density matrix in the following form:

$$\rho_{\nu\nu'} = \rho^0(\nu) \delta_{\nu\nu'} + \delta\rho_{\nu\nu'} e^{-i\omega t}. \quad (2.1)$$

If we are interested in linear problems we can write down for the non-equilibrium correction to the density matrix the following approximate equation (cf.<sup>[4]</sup>):

$$\{\hbar\omega - \varepsilon(\nu') + \varepsilon(\nu)\} \delta\rho_{\nu\nu'} + \{\rho^0(\nu') - \rho^0(\nu)\} \cdot \left\{ -\frac{1}{c} \sum_{\mathbf{q}} \delta\mathbf{j}_{\nu'\nu} \delta\mathbf{A}_{\mathbf{q},\omega} + \sum_{\nu_1\nu_2} F_{\nu'\nu}^{\nu_1\nu_2} \delta\rho_{\nu_1\nu_2} \right\} = J_{\nu'\nu}^{\text{ext}}. \quad (2.2)$$

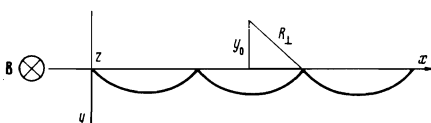


FIG. 1.

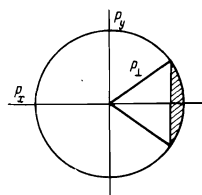


FIG. 2.